



HAL
open science

Surface modification of 5083 Aluminum-Magnesium induced by marine microorganisms

Julien Jaume, Maria Joao Marques, Marie-Line Délia, Régine Basséguy

► To cite this version:

Julien Jaume, Maria Joao Marques, Marie-Line Délia, Régine Basséguy. Surface modification of 5083 Aluminum-Magnesium induced by marine microorganisms. *Corrosion Science*, 2022, 194, pp.109934. 10.1016/j.corsci.2021.109934 . hal-03440993

HAL Id: hal-03440993

<https://hal.science/hal-03440993v1>

Submitted on 22 Nov 2021

HAL is a multi-disciplinary open access archive for the deposit and dissemination of scientific research documents, whether they are published or not. The documents may come from teaching and research institutions in France or abroad, or from public or private research centers.

L'archive ouverte pluridisciplinaire **HAL**, est destinée au dépôt et à la diffusion de documents scientifiques de niveau recherche, publiés ou non, émanant des établissements d'enseignement et de recherche français ou étrangers, des laboratoires publics ou privés.



[Open Archive Toulouse Archive Ouverte](#)

OATAO is an open access repository that collects the work of Toulouse researchers and makes it freely available over the web where possible

This is an author's version published in: <http://oatao.univ-toulouse.fr/28536>

Official URL : <https://doi.org/10.1016/j.corsci.2021.109934>

To cite this version:

Jaume, Julien^{ORCID} and Marques, Maria Joao^{ORCID} and Délia, Marie-Line^{ORCID} and Basséguy, Régine^{ORCID} *Surface modification of 5083 Aluminum-Magnesium induced by marine microorganisms*. (2021) *Corrosion Science*, 194. 109934. ISSN 0010-938X

Any correspondence concerning this service should be sent to the repository administrator: tech-oatao@listes-diff.inp-toulouse.fr

Surface modification of 5083 Aluminum-Magnesium induced by marine microorganisms

J. JAUME^a, M.J.F. MARQUES^{a,b}, M.L. DÉLIA^a, R. BASSÉGUY^a

a. Laboratoire de Génie Chimique, Université de Toulouse, CNRS, INPT, UPS, Toulouse, France

b. LMR – Laboratório de Materiais e Revestimentos, LNEG – Laboratório Nacional de Energia e Geologia, Lisboa/Portugal

Abstract

The influence of microorganisms from a salt marsh in the surface modification of 5083 aluminium alloy (Al-Mg) in seawater was evaluated. An immersion test performed for 50 days in biotic and abiotic conditions, with electrochemical monitoring and surface/cross-section characterization by SEM/EDX and TEM after exposure, showed that microorganisms induced the formation of a homogenous layer on the Al-Mg surface. This layer, which proved to be composed of a double-structure: a dense, amorphous inner layer and a more porous outer layer, was demonstrated to influence the corrosion resistance of the Al-Mg alloy in seawater.

1. Introduction

Aluminium alloys are widely used for marine craft because of their high corrosion resistance, lightness, easy workability and recyclability [1]. The 5000 series Al-Mg alloys are particularly recommended for this purpose. However, the use of aluminium alloy does not make processing and maintenance unnecessary in a marine environment [2]. Under certain circumstances, even the most corrosion-resistant aluminium alloys may develop pitting corrosion as well as galvanic corrosion in seawater. Although a thin protective oxide film forms spontaneously on the surface of the aluminium alloy, chlorides are able to break this layer and thus allow corrosion to spread [3–5].

Furthermore, materials exposed to the natural environment are covered by microorganisms forming a biofilm on their surface. The biofilm is made up of a community of microorganisms embedded in extracellular polymeric substances (EPS), attached to a solid surface [6,7]. In the case of metallic materials susceptible to corrosion, the presence of biofilm can accelerate their degradation. This phenomenon is known as MIC, for Microbiologically Influenced Corrosion [8–11], and is particularly promoted in seawater, which is an aggressive medium due to the high concentration of chloride and the presence of a broad indigenous microbial flora. Numerous microorganisms are known to catalyze corrosion reactions include metal-reducing bacteria, metal-depositing bacteria, acid-producing bacteria, and fungi [8,9]. The most common are mentioned below. Under aerobic conditions, some microorganisms, like *Pseudomonas aeruginosa*, which produces the pyocyanin mediator, are able to catalyze the oxygen reduction [12,13] via direct (DET) or mediated electron transfer (MET) [14]. For oxygen reduction catalysis, it has been shown that a multispecies biofilm is more efficient than a single species [12,15]. Moreover, the diversity of the biofilms that develop in the marine environment depends on the nature of the immersed material. For example, the dominant genera have been shown to differ when samples are made of copper, steel or aluminium [16], which will certainly lead to various MIC mechanisms.

Most MIC studies in an anaerobic environment have focused on Sulfate-Reducing Bacteria (SRB), which lead to the formation of FeS that catalyzes water reduction on steel [9]. In the case of Al alloys, MIC caused by SRB in seawater has been studied on 5052 aluminium alloy. Localized corrosion was observed with and without SRB because of the presence of chloride ions in seawater, but pitting corrosion was greatly enhanced by metabolites (acid or other) produced by the microorganisms [17].

MIC on aluminium alloys has also been reported in other environments, such as aircraft tanks, where the 2024 aluminium alloy was attacked by a fungus, *Hormoconis resiniae*, capable of growing on a hydrocarbon-rich substrate [18]. Several studies have pointed out the relevant fact that microorganisms involved in MIC act synergistically in multi-species biofilm, causing more damage than when only a single species is present [9,19,20].

Some microorganisms are also able to inhibit corrosion. This phenomenon is known as MICI, for Microbiologically Influenced Corrosion Inhibition [21–23]. Mechanisms inducing MICI are various, for example, in the formation of a protective layer, *Pseudomonas putida* RSS can produce a stable Fe-EPS complex inducing the formation of a vivianite layer protecting mild steel from corrosion [24]; *Geobacter sulfurreducens* is known to reduce Fe(III) to Fe(II), also leading to the formation of a vivianite layer on steel in a medium containing phosphate compounds [23]. A recent study showed the protective effect of *Bacillus subtilis* on 2024 aluminium alloy in a marine environment through the formation of a layer of $\text{CaMg}(\text{CO}_3)_2$ [25], while another mechanism consists in the depletion of oxygen at the metal surface: aerobic bacteria such as *Pseudomonas fragi* can inhibit the corrosion of steel by consuming oxygen [26]. A long term immersion test shown the beneficial effect of the biofouling that limited the exfoliation corrosion [27]. However, MICI is highly dependent on the nature of the material, for example, *Bacillus mycoides* causes MIC on zinc, MICI on aluminium and has no effect on steel [28]. It is also noteworthy that most of the research reported on MICI concerns laboratory studies involving only a single species; generally, no multi-species consortium was used. Nevertheless, a study from a National Joint Industry Project on corrosion protection for aluminium boats showed that a protective layer against corrosion developed on 5083 aluminium alloy immersed in an estuarine environment (field conditions) for 2 and 3 years [29]. This protective coating, formed as result of interactions between microorganisms and the metal, was characterized by SEM/EDS and electrochemical techniques [30] and the corrosion resistance behavior was evaluated by an accelerated aging test [31]. This work suggests that understanding the mechanism through which the MICI phenomena linked to a multi-species consortium increase the Al-Mg corrosion resistance in marine environment could be envisaged as an innovative way of considering the development of anti-corrosion solutions. In this context, the present work is the first step in an attempt to reproduce the protective phenomenon in controlled laboratory conditions using a multi-species source of microorganisms drawn from a salt marsh. The salt marsh is interesting for its wild microbial population [32,33] that will be selected and will develop according to the conditions to which it is exposed [34,35]. For instance, salt marsh has already been studied for its ability to grow a biofilm catalyzing oxygen reduction on a carbon felt electrode [34]. This catalytic property was correlated to the presence of Gammaproteobacteria strain(s) related to *Thiohalobacter thiocyanaticus*, which were considerably enriched in the best performing biocathodes. Moreover, a stringent selection of two microbial genera of *Marinobacter spp* and *Desulfuromonas spp* was observed when salt marsh was used to form bioanodes [35].

The aim of the present work is to study the influence of the marine microbial population on the corrosion behavior of Al-Mg alloy immersed in seawater in the laboratory, using short time scales. For this purpose, electrochemical measurements were performed during 50 days on 5083-H111 aluminium alloy immersed in biotic conditions with active microorganisms from the salt marsh and in an abiotic condition using autoclaved salt marsh. At the end of the exposure period, the amount of dissolved aluminium in solution was measured by ICP-AES analysis and Al-Mg alloy samples exposed in biotic and abiotic conditions were examined and characterized by scanning electron microscopy (SEM) with energy dispersive X-Ray analysis (EDX). Additionally, a detailed study of the morphological, structural and local chemical composition of the layer formed at the surface of the Al-Mg alloy exposed to marine microbial influence was made using TEM examination of a cross-section.

2. Materials and methods

2.1. Electrode materials

Electrodes were made of aluminum-magnesium alloy 5083-H111. Their dimensions were 4 cm x 5 cm with a thickness of 0.7 cm. Four samples of the Al-Mg alloy were analyzed by WDXRF spectrometry (Table 1) to ensure compliance with the European standard prEN 573-3:2018 [36].

Element	Mean value (wt %)	Standard (wt %)
Magnesium	4.4 ± 0.08	4.0 – 4.9
Manganese	0.64 ± 0.1	0.40 – 1.0
Iron	0.24 ± 0.05	0.4
Silicon	0.26 ± 0.08	0.4
Chromium	0.09 ± 0.02	0.05 – 0.25
Zinc	< 0.01	0.25
Titanium	0.02 ± 0	0.15
Copper	< 0.02	0.10
Aluminium	Remainder	Remainder

Table 1 : Elemental composition (wt%) of samples from the 5083alloy and comparison with Standard EN 573

Al-Mg alloy electrodes were cut from a larger plate by electro-erosion. Before use, they were cleaned by spraying first ethanol then acetone on the electrode and drying with a soft paper towel.

2.2. Immersion conditions

Natural seawater was used as the liquid medium to study the corrosion behavior of the aluminium alloy. Salt marsh was used as the source of microorganisms. Seawater and salt marsh were harvested near the coast at Gruissan, France. The composition of the salt marsh has been shown not to vary over time [35]. Before use, salt marsh was stored to allow the solid sludge sediments to settle at the bottom of the container, leaving the liquid part above.

Different mixtures of seawater and salt marsh (vol/vol) (Figure 1) were prepared, with a total volume of 600 mL:

- Biotic condition 1: Seawater 90% + Solid sludge of salt marsh 5% + Salt marsh liquid 5%.
- Biotic condition 2: Seawater 90% + Solid sludge of salt marsh 10%.
- Abiotic condition: Seawater 90% + Sterilized solid sludge of salt marsh 10%.

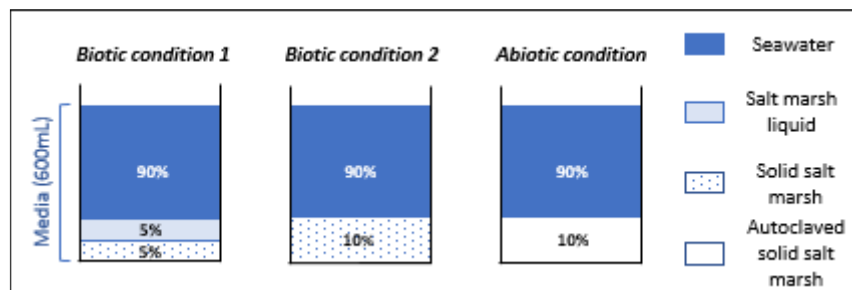


Figure 1 : Different immersion conditions

Two biotic conditions, using various amounts of liquid and solid sludge from the salt marsh, were considered to determine the influence of the different populations. It was assumed that the liquid part contained a higher proportion of aerobic bacteria than the solid sludge part.

To obtain the abiotic condition, the salt marsh was sterilized by autoclaving for 20 minutes at 121°C.

Seawater was not sterilized, as a few liters of seawater do not contain enough endogenous microorganisms to develop an electroactive marine biofilm in a closed container [37] and consequently to have an impact on the corrosion behavior. Indeed, preliminary tests (not shown) using sterilized seawater by autoclave or 0.2 μ m filter, leads to the same results as the abiotic condition used here.

2.3. Experimental setup

The reactors consisted of borosilicate glass flasks with a three-electrode system (Figure 2):

- The working electrode (4 x 5 x 0.7 cm) made of aluminium alloy 5083-H111 (see part 2.1.) was placed in the center of the bottle, on a plastic support.
- The counter-electrode consisted of two iridium-tantalum dimensionally stable anodes (DSA from Magneto) with a surface area of 5 cm x 3 cm, placed on either side of the working electrode. This setup ensured that the electrochemical conditions were the same on both sides of the aluminium alloy electrode.
- A saturated calomel reference electrode (SCE)
- A frit nozzle, connected to an aquarium pump, aerated the medium continuously. The air passed through a pre-bubbler beforehand to humidify the air and thus avoid evaporation in the reactor.

The working electrode was immersed in this medium for 50 days.

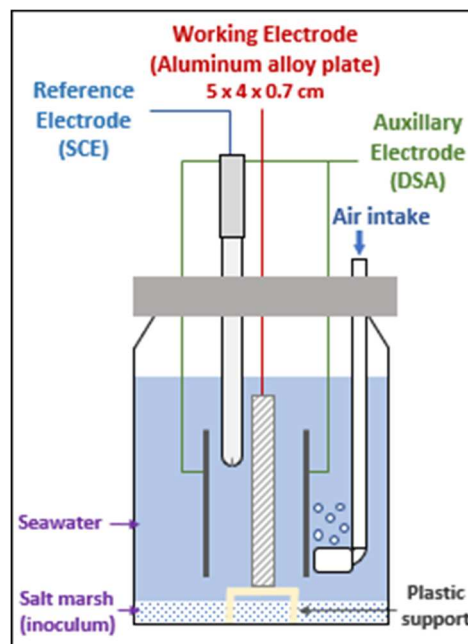


Figure 2 : Experimental setup of the three-electrode system

2.4. Electrochemical experimentation

To perform electrochemical measurements, the experimental setup was connected to a Biologic VMP2 or a Gamry 600 potentiostat with an ECM8 Electrochemical Multiplexer.

The open circuit potential (OCP) was recorded when no other electrochemical measurements were being conducted.

Linear sweep voltammetry (LSV) was performed after 2 hours of immersion and then every two days. The potential of the LSV started from the open circuit potential (OCP) and varied to -0.020 V/OCP with a scan speed of 0.167 mV/s. The LSV was performed only on the cathodic side in order not to alter the Al-Mg electrode when applying an anodic potential. Thus, the inverse of the polarization resistance, $1/R_p$, was calculated using the linear regression on the LSV in the vicinity of the OCP.

2.5. ICP-AES analysis

After 50 days of immersion, the liquid medium was sampled from the glass flasks and analyzed by ICP-AES with an Ultima Expert (Horiba) at the wavelength of 237.312 nm to determine the amount of dissolved aluminium present in each medium. The samples were diluted 5 times with ultrapure water for analysis.

2.6. SEM/EDX characterization

After 50 days of immersion, the Al-Mg electrodes were carefully rinsed with flowing distilled water and dried under controlled atmospheric conditions before surface and cross-section preparation for SEM/EDX characterization. The observations were performed using a SEM TM3000 (Hitachi) scanning electron microscope paired with a SwiftED3000 EDX (Hitachi) energy dispersive X-ray spectrometer to perform elementary chemical analysis.

The metallographic samples were prepared using a cold mounting epoxy resin. The cross-sections were then ground (SiC abrasives with several grain sizes up to 1000 grit) and polished (diamond paste up to 1 μm grain size). All prepared samples, surface and cross section, were metallized with gold (Au) prior to SEM observation in order to reduce charging effects.

2.7. TEM analysis of Al-Mg alloy after biotic immersion

Cross-section TEM preparation by focused ion beam (FIB) extraction was performed for a detailed characterization in terms of morphology, structure and chemical composition of the protective layer formed on the Al-Mg alloy surface exposed to marine microbial influence.

A thin cross-section lamella, as small as 15 μm \times 10 μm , was obtained from the Al-Mg electrode immersed in biotic condition 1 using a FIB FEI 600i (HELIOS), following a dedicated sample preparation procedure. The TEM investigation, carried out with a JEM 2100F (JEOL) coupled to energy dispersive X-ray spectrometer EDX (Bruker), included TEM imaging, EDX analysis with acquisition of elemental maps and selected area electron diffraction (SAED) patterns.

3. Results

3.1. Electrochemical study

Experiments were carried out in duplicate for each of the three media available. The open circuit potential (OCP) was measured for 50 days (Figure 3). The OCP remained stable in the abiotic condition (around -0.7 V/SCE), whereas a drop of the recorded potential from -0.8 to -1 V/SCE was observed after around 5 days for experiments in presence of active salt marsh (biotic conditions 1 and 2). The LSV data were processed to obtain the inverse of the polarization resistance, $1/R_p$, which varied in the same way as the exchange current density and gave an estimation of the surface reactivity. In our experiments, it was not possible to access the value of i_{corr} from $1/R_p$ because the conditions for determining the Tafel constants were not met. However, since all aluminium alloy electrodes had the same dimensions, it was possible to compare the $1/R_p$ among them and thus to obtain the evolution of the exchange current during the 50 days of immersion (Figure 4):

- At the very beginning of immersion, a high corrosion current was observed in media containing the active salt marsh (biotic conditions 1 and 2). A high corrosion rate was expected when the aluminium alloy electrode was immersed in a high chloride environment. However, the trend was quickly reversed and the exchange current decreased rapidly, with $1/R_p$ settling down to around $1 \cdot 10^{-4} \text{ Ohm}^{-1}$ on day 5. The decrease in $1/R_p$ at 5 days for active salt marsh might be related to the decrease in the open circuit potential observed on the same day (Figure 3).

- In experiments with sterilized salt marsh, $1/R_p$, that represent the corrosion current, first increased to $7.8 \Omega^{-1}$, remained at a high value for at least 9 days, and then decreased to stabilize after 20 days at the same value as in non-sterile conditions. However, this decrease was not related to a drop of potential as seen with active salt marsh (Figure 3).

From this electrochemical study, it was established that there were two different behaviors depending on whether the Al-Mg alloy electrode was immersed in presence of active or sterilized salt marsh.

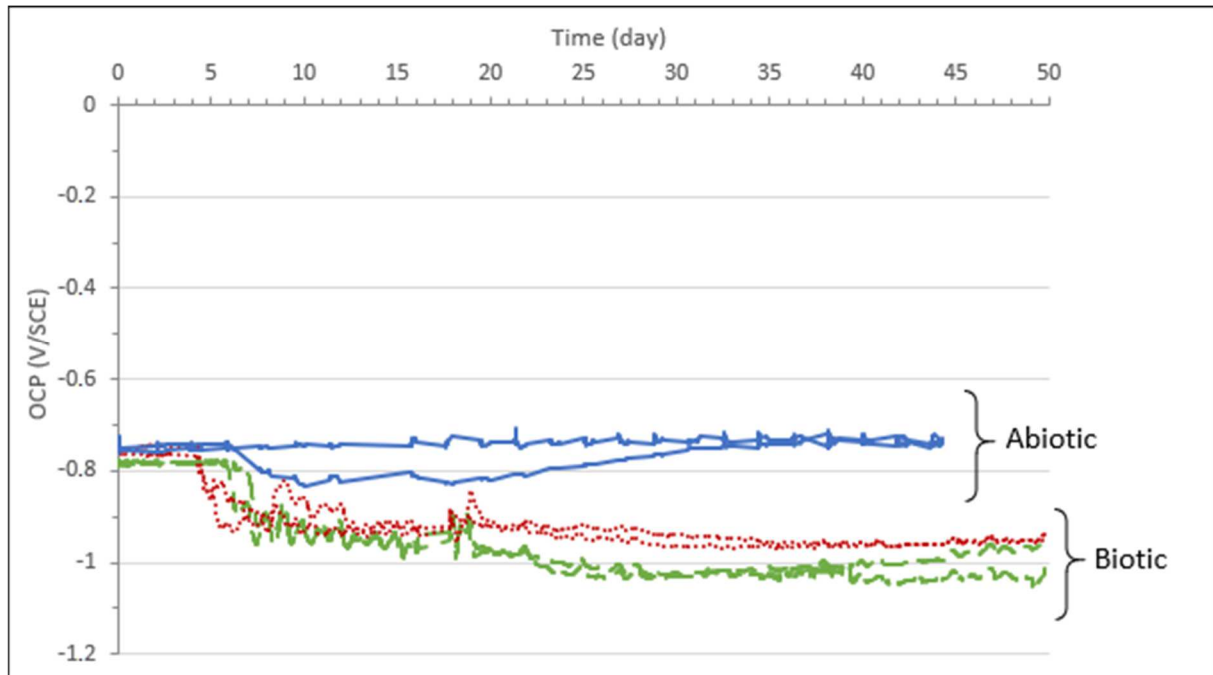


Figure 3 : Open circuit potential (OCP) recorded during 50 days of immersion for biotic condition 1 (green dashes), biotic condition 2 (red dots) and abiotic condition (blue solid line)

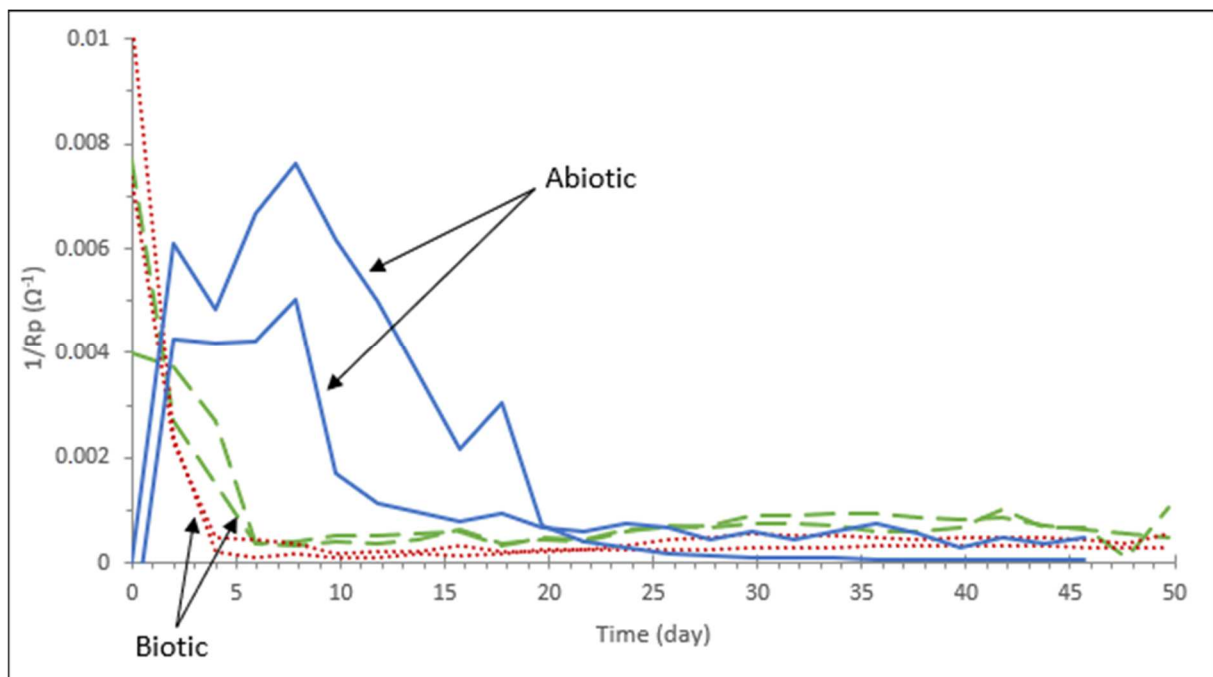


Figure 4 : Evolution of $1/R_p$ during 50 days of immersion for biotic condition 1 (green dashes), biotic condition 2 (red dots) and abiotic condition (blue solid line)

3.2 ICP-AES analysis

The results obtained by ICP-AES for the amount of aluminium dissolved after 50 days of immersion in the different conditions tested are shown in Table 2. The concentration of dissolved aluminium was higher for the abiotic condition than with the biotic conditions. The greatest difference was observed between biotic condition 1 and the abiotic condition, where the amount of aluminium measured was reduced by a factor of around 4.6.

Sample	Dissolved aluminium
Biotic condition 1	130 µg/L
Biotic condition 2	470 µg/L
Abiotic condition	610 µg/L

Table 2 : Dissolved aluminium analyzed by ICP-AES in the seawater after 50 days of immersion.

These results are consistent with the $1/R_p$ values observed in Figure 4. The lower quantity of dissolved aluminium found in biotic conditions 1 and 2 can be related with the low corrosion currents reached very early, after only 5 days. The high corrosion current observed over several days in the abiotic condition (Figure 4) was correlated with the higher amount of dissolved aluminium measured by ICP.

3.3. SEM/EDX characterization

Figure 5 shows the visual aspect of the Al-Mg electrode surface before and after 50 days of immersion in biotic and abiotic environments. Before immersion, the morphology presented by the aluminium alloy was the result of the surface preparation by a grinding process (Figure 5A). After 50 days of exposure, it was possible to observe a visible surface modification of the aluminium alloy electrodes in the different testing conditions.

After immersion of the aluminium alloy in biotic condition 1 (Figure 5.C), a homogeneous black deposit covered the whole surface. A similar phenomenon was observed on the surface of the electrode immersed in biotic condition 2 (Figure 5D) but some areas of the electrode were less covered. Finally, the electrode immersed in the abiotic condition (Figure 5B) showed a more significant corrosion attack with many white deposits distributed over the entire surface.

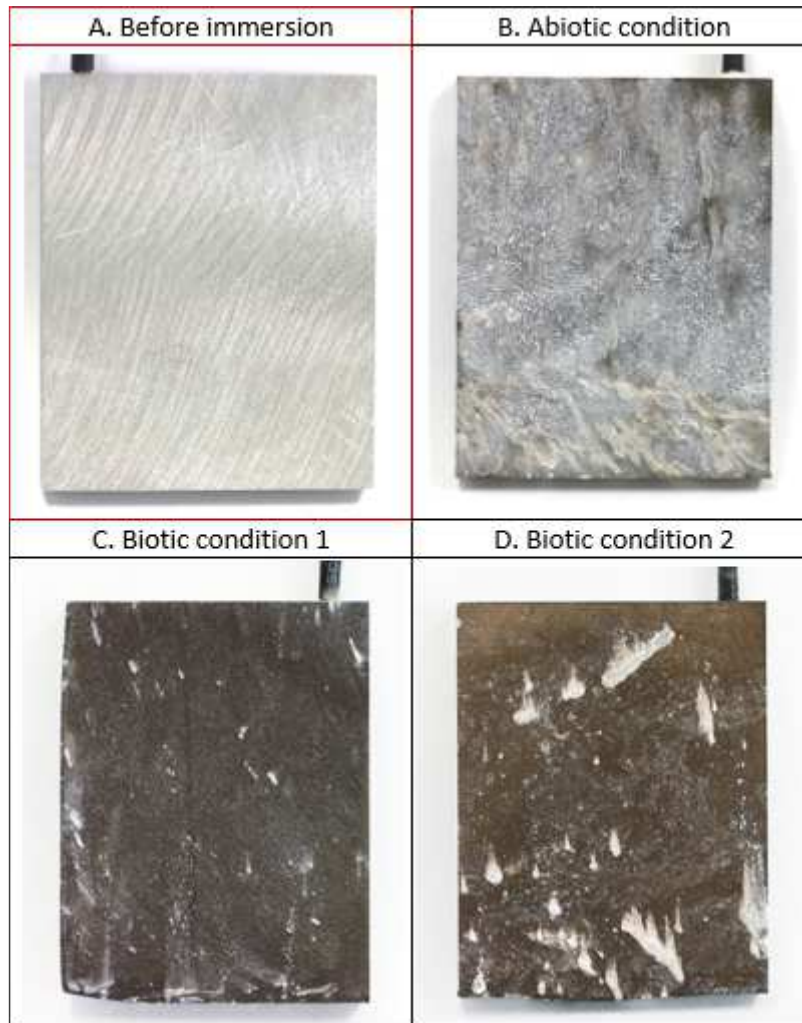


Figure 5 : Photographs of aluminium alloy before and after 50 days of immersion in various conditions

After visual inspection, the surface and the cross-section of these samples were observed and analyzed by SEM/EDX.

3.3.1 Biotic condition 1

Figure 6 shows deposit morphology and its distribution on the Al-Mg alloy surface in biotic condition 1, revealing a homogeneous distribution.

SEM observation of the cross-section confirmed that a thin layer was formed along the aluminium alloy surface with a thickness distribution that was not totally uniform (Figure 7). Figure 7A and 7B correspond to areas with low surface roughness, where presence of the homogenous layer was observed. Figure 7C (zoom in on Figure 7A) shows the good adhesion of the layer to the aluminium alloy surface and its ability to slightly decrease the surface roughness. Figure 7D corresponds to an area with higher surface roughness where, despite its heterogeneous thickness, the presence of the layer on the surface of the Al-Mg alloy is still visible. The cross-sectional observation of the sample confirmed the absence of localized attack on the aluminium alloy.

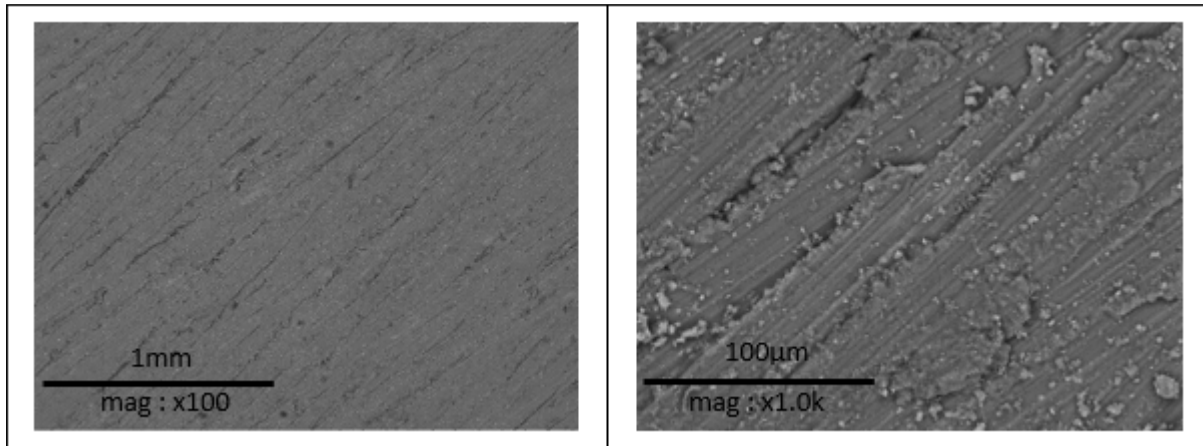


Figure 6 : Surface SEM observation of a sample immersed in *biotic* condition 1

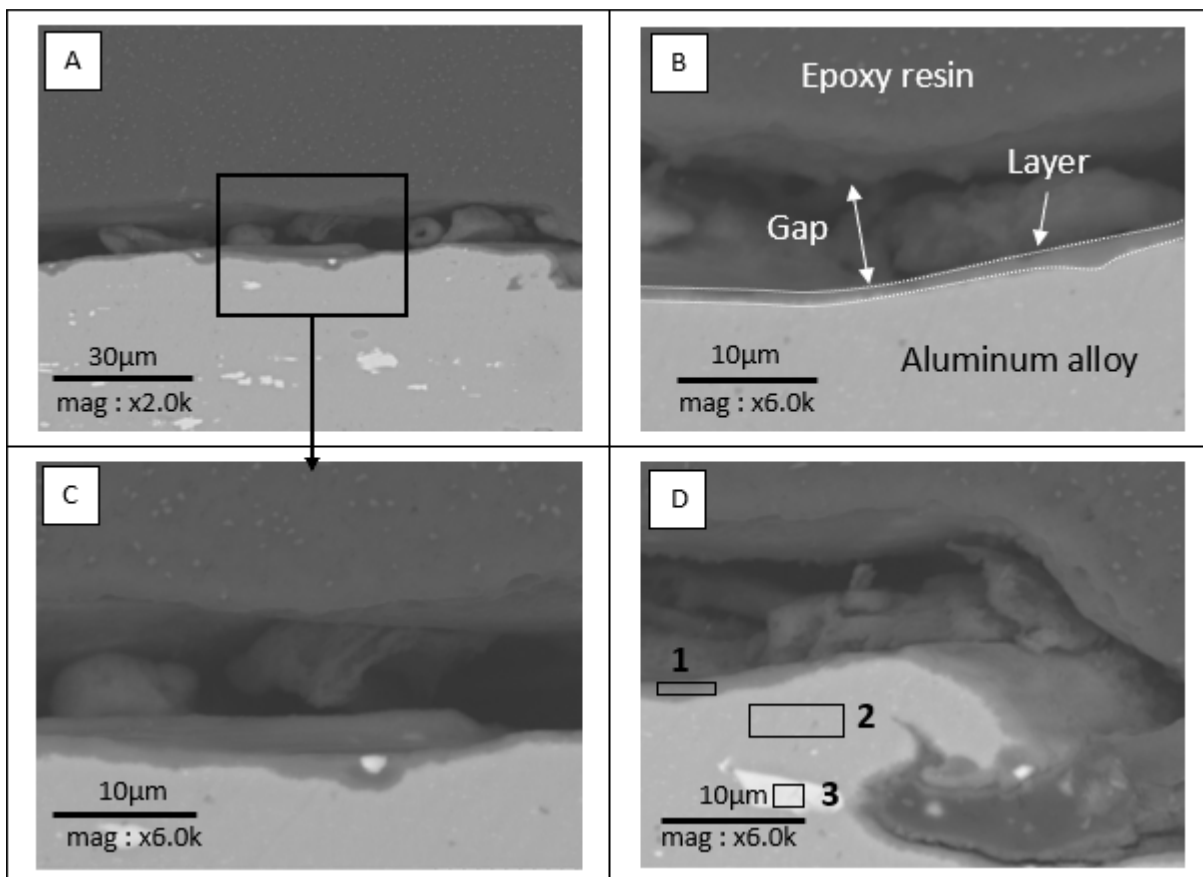


Figure 7 : Cross-sectional SEM observation of a sample immersed for 50 days with *biotic* condition 1. A and B reflect areas with less roughness than D. Framed areas on image D were analyzed by EDX and associated spectra are grouped in Figure 8

EDX analysis was performed on the areas shown on Figure 7D and the associated spectra are presented in Figure 8.

Spectrum 1 shows that the layer formed on the surface of the aluminium alloy is composed mainly of aluminium and oxygen but also contains significant amounts of silicon, carbon and magnesium. A residual presence of calcium was also detected.

Spectrum 2, performed at the matrix of the Al-Mg alloy, reveals the proportion of aluminium and magnesium expected for the Al-Mg alloy under study (Table 1).

Spectrum 3 corresponds to an intermetallic particle inside the Al-Mg matrix. The main elements detected are aluminium, iron and manganese, with some chromium.

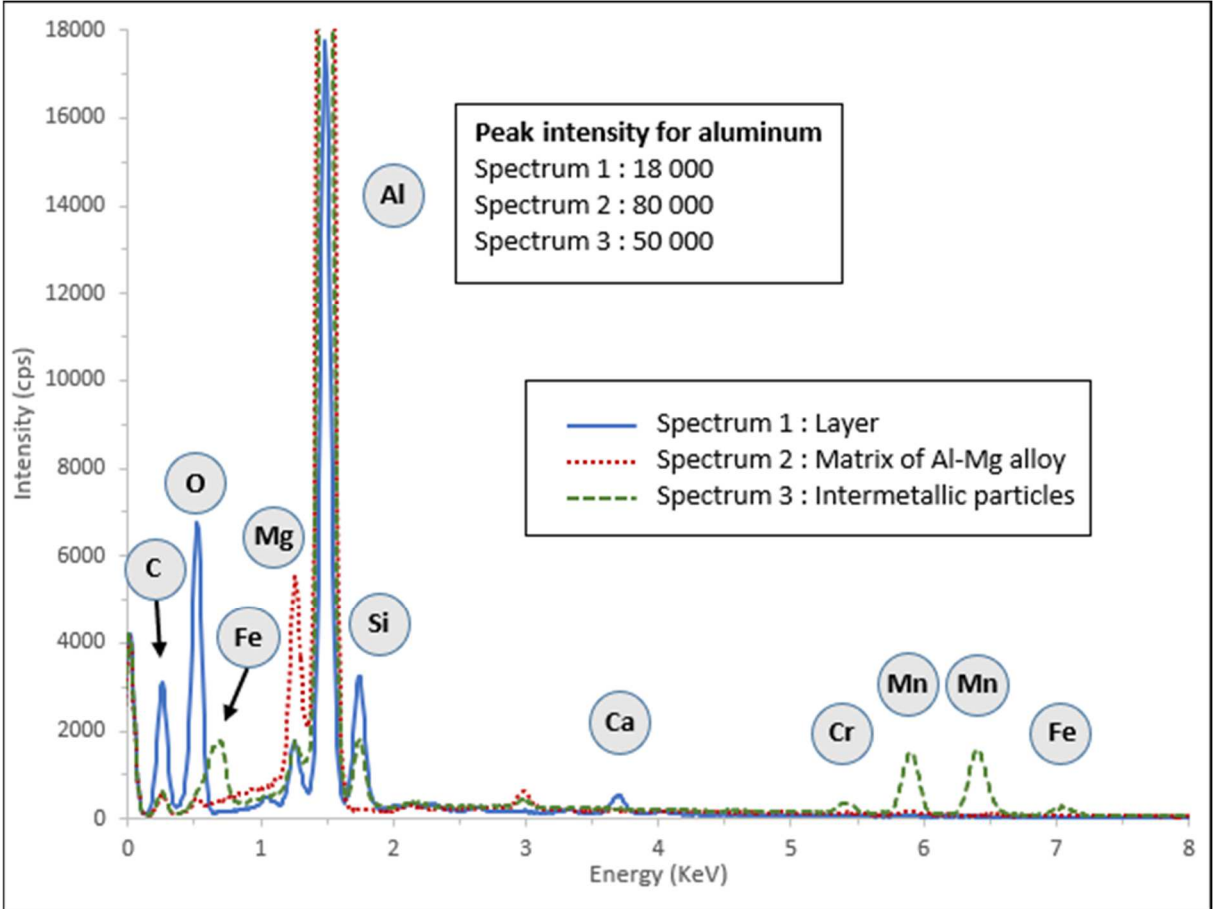


Figure 8 : EDX analysis of the sample in biotic condition 1, for areas framed in Figure 7D: zone 1 (Layer), zone 2 (Matrix of Al-Mg alloy) and zone 3 (Intermetallic particles)

3.3.2 Biotic condition 2

The SEM observations of the Al-Mg surface modification after 50 days of immersion in biotic condition 2 showed similarities with the observations performed on the aluminium alloy exposed in biotic condition 1 but, in this case, the layer presented less homogeneous coverage of the surface (Figure 9). The cross-section observation confirmed the presence of the layer on the Al-Mg surface which, although showing a relatively homogeneous distribution, revealed some discontinuities where localized aluminium alloy corrosion was observed (Figure 10).

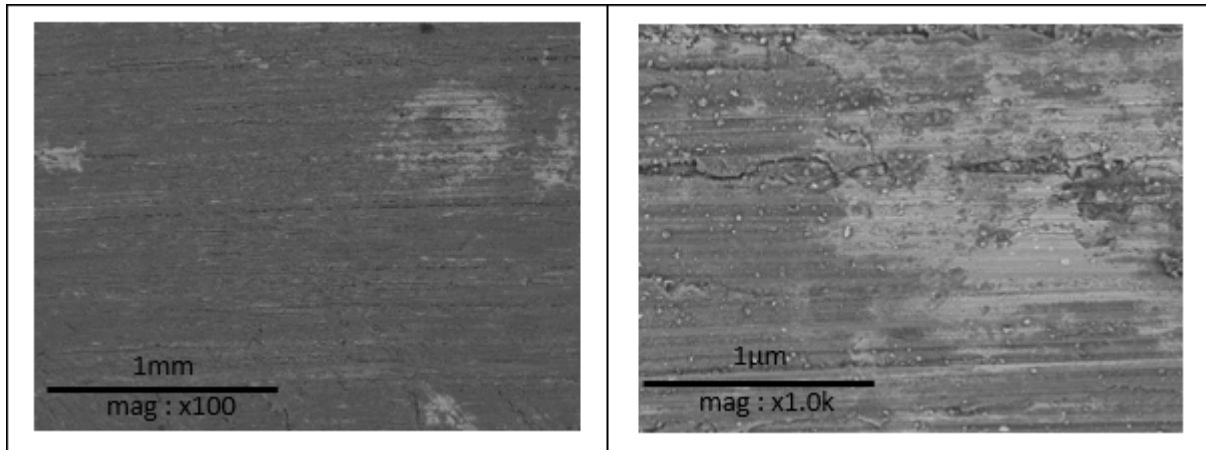


Figure 9 : Surface SEM observation of a sample immersed in **biotic** condition 2.

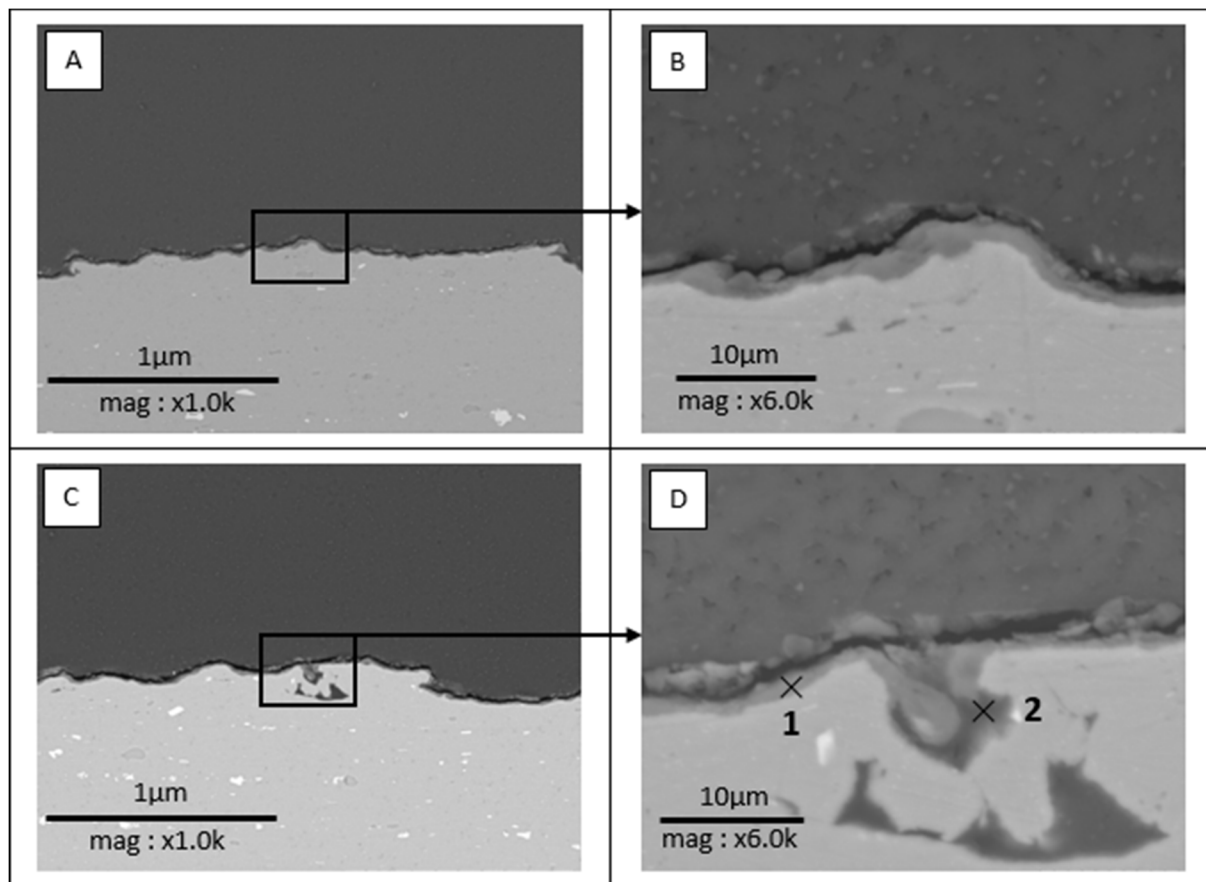


Figure 10 : Cross-sectional SEM observation of a sample immersed for 50 days with **biotic** condition 2. Images A and B show the shape of the layer, while images C and D reveal a defect in this layer. Areas indicated by crosses on image D were analyzed by EDX.

EDX analysis was performed on the areas indicated by crosses in Figure 10D. The corresponding spectra are compared in Figure 11.

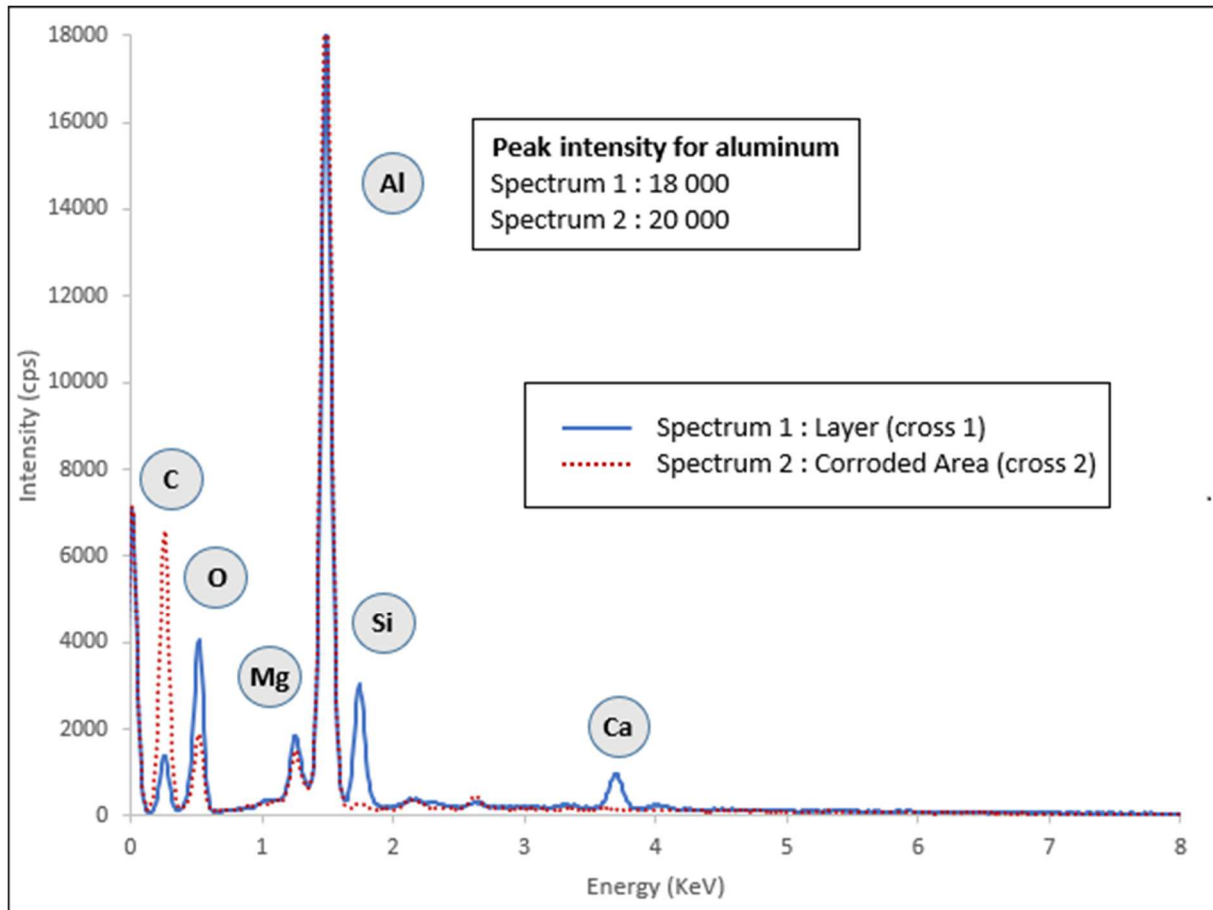


Figure 11 : EDX analysis of the sample in *biotic* condition 2, Figure 10D, spectrum at cross 1 (Layer) and spectrum at cross 2 (Corroded area)

Spectrum 1 shows that the layer above the Al-Mg matrix was composed mainly of aluminium, oxygen, silicon, and magnesium, with some carbon and calcium. This spectrum and that of the layers developed under biotic condition 1 are close. Layers grown under biotic conditions 1 and 2 had similar compositions.

Spectrum 2 shows the products of localized corrosion, mainly aluminium, oxygen and magnesium. The difference between this spectrum and that of the layer (spectrum 1) is the absence of silicon and calcium.

3.3.3 Abiotic condition

The Al-Mg samples immersed in abiotic conditions showed different behavior from that observed under biotic conditions. The SEM observations reveal a surface randomly covered with deposits, in which the initial surface roughness associated with the grinding process is still visible (Figure 12). Through cross-sectional observation (Figure 13), it was possible to verify the beginning of the corrosion process of the aluminium alloy, which seems to develop, not in the form of pitting, but in planes parallel to the surface. When present in a more advanced state, this type of corrosion is known as exfoliation corrosion.

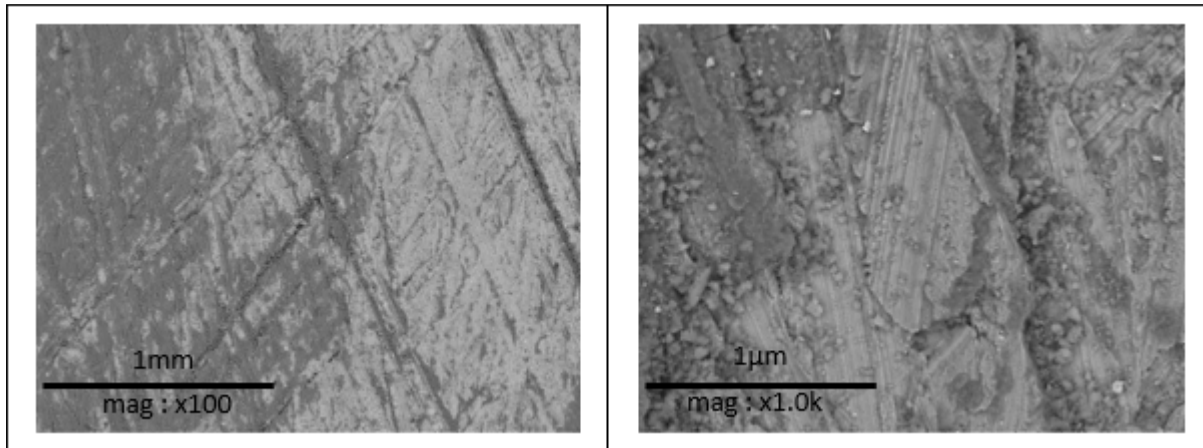


Figure 12 : Surface SEM observation of a sample immersed in *abiotic* condition

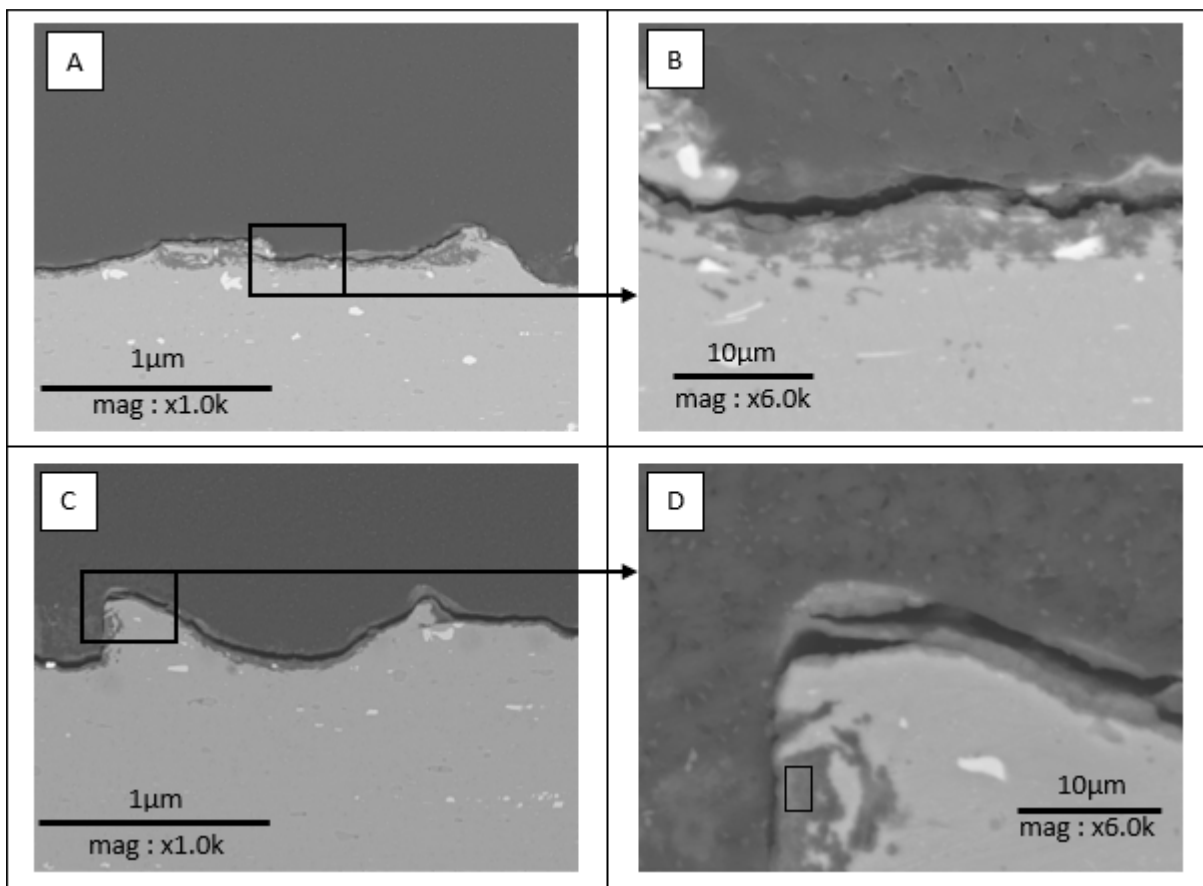


Figure 13 : Cross-sectional SEM observation of a sample immersed for 50 days in *abiotic* condition. A and C show corrosion at the surface of the aluminium alloy. The framed area on image D was analyzed by EDX.

An EDX analysis was performed (Figure 14) on this sample, at the corroded area framed in Figure 13D. The corrosion products were mainly composed of aluminum, oxygen, carbon, magnesium, and silicon, with some sulfur and calcium.

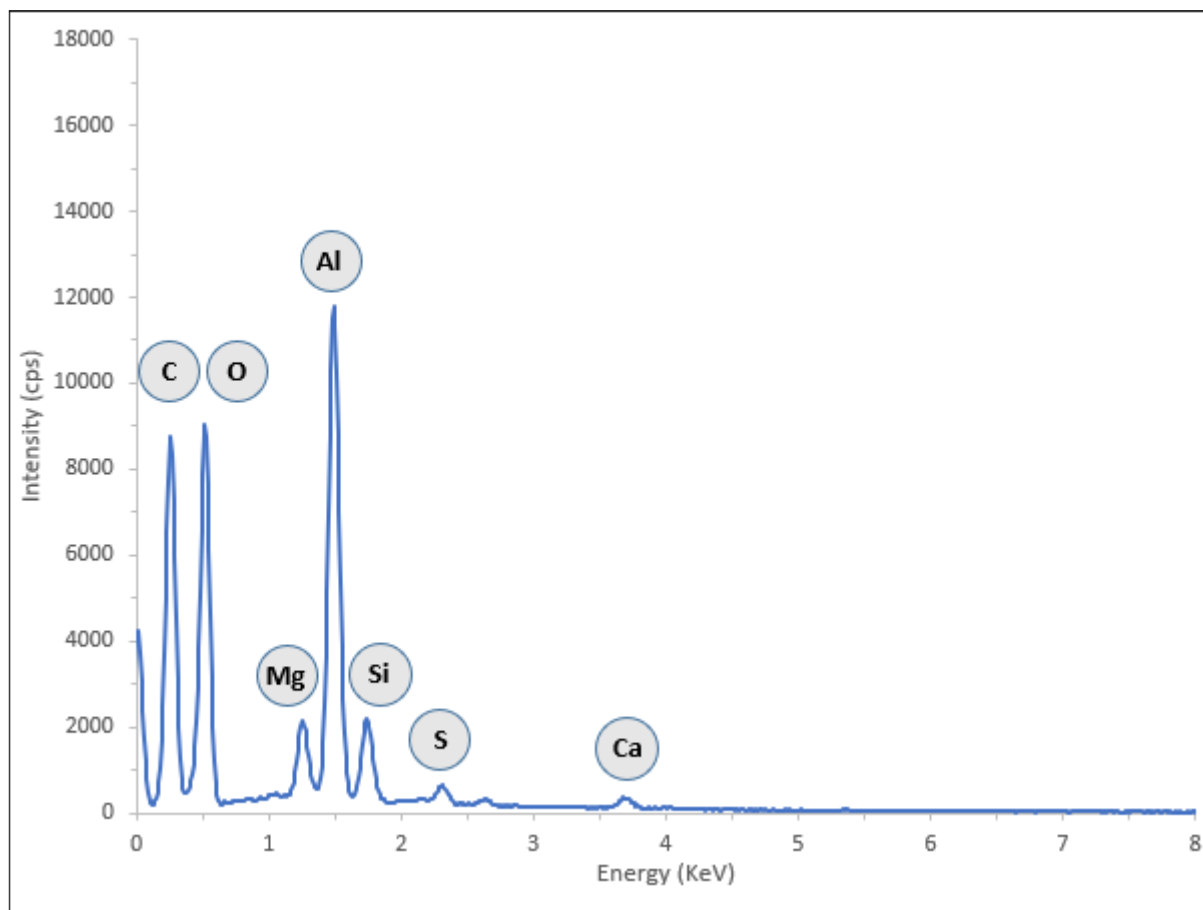


Figure 14 : EDX analysis of the sample immersed in *abiotic* condition, on the framed zone of Figure 13D

3.4. TEM analysis of Al-Mg exposed to marine microbial influence (*biotic condition 1*)

A detailed characterization of the layer formed on the Al-Mg surface immersed in biotic condition 1, which had an average thickness of about 1 μm , was performed by TEM with a cross-section sample obtained by FIB extraction (Figure 15A). The layer revealed a two-layered structure, comprising a dense inner layer not uniformly distributed on the substrate, with an average thickness of 553 nm (standard deviation of 250 nm), and a porous outer layer on top, showing a homogeneous distribution with an average thickness of 478 nm (standard deviation of 87 nm). In Figure 15B, it can be seen that the interface between the aluminium alloy and the inner layer has no gaps, showing excellent adhesion. The same behavior is observed at the interface between the inner and outer layers, despite their morphological differences.

The X-ray element maps and the distribution profile of the elements drawn up for the two layers (Figure 16 and Figure 17) indicate that the differences of morphology observed in the two layers are also associated with their distinct elementary compositions. The porous outer layer reveals a more significant presence of magnesium (Mg) than the inner, dense layer, which presents higher aluminium (Al), oxygen (O), silicon (Si) and calcium (Ca) contents. Notwithstanding these results, it should be noted that the apparently lower density of the outer layer compared to the inner layer may have an influence on the detection of some chemical elements, since a smaller amount of X-rays will be emitted from the same analyzed volume.

Additionally, TEM diffraction mode was used for the structural characterization of the two layers (Figure 18). The selected area electron diffraction (SAED) pattern revealed that the dense layer was amorphous (absence of spots in the SAED pattern, Figure 18B), while the electron beam did not interact with enough matter in the porous layer for any information to be obtained about its structure.

In the case of the Al-Mg alloy, the appearance of spots in the SAED pattern corroborated the presence of crystalline phases (Figure 18C).

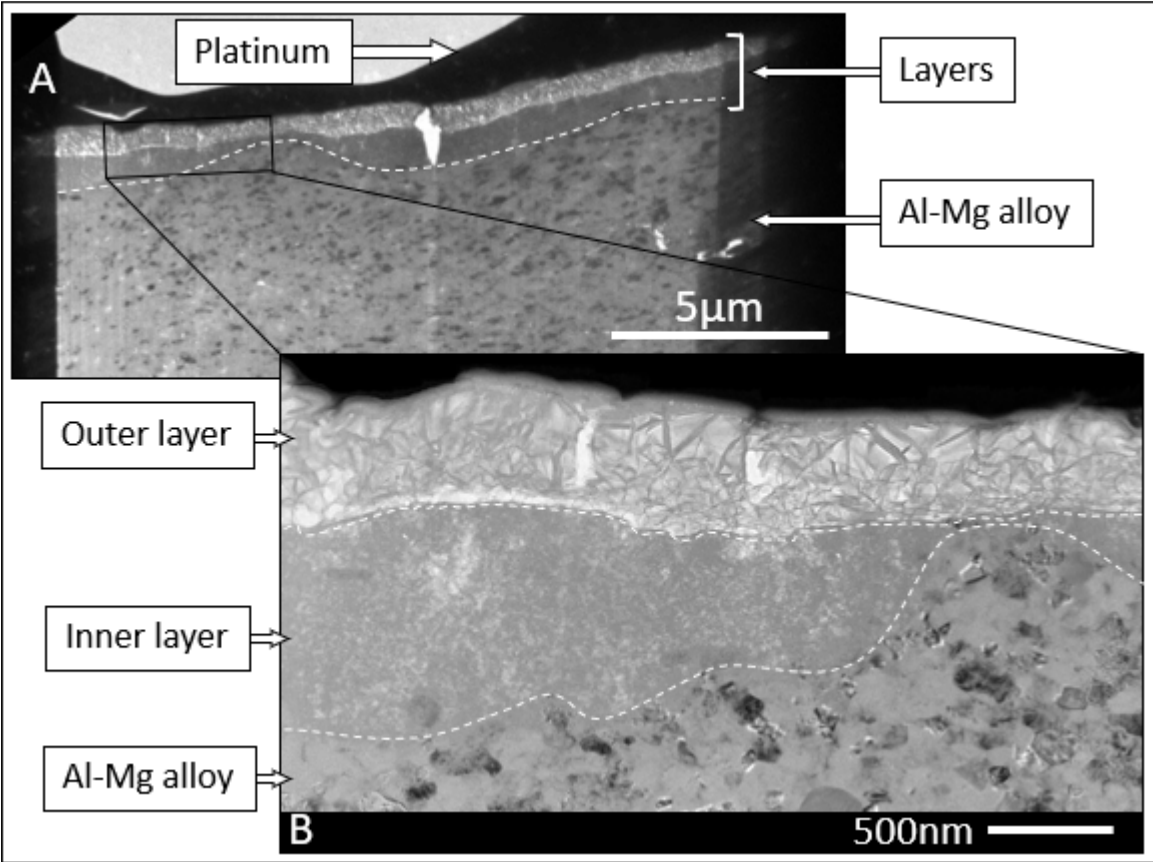


Figure 15 : Cross-sectional bright-field TEM image of the layer formed at the Al-Mg electrode surface after 50 days of immersion in biotic condition 1. (A) Detail showing a two-layer structure: an inner dense layer and outer porous layer (B).

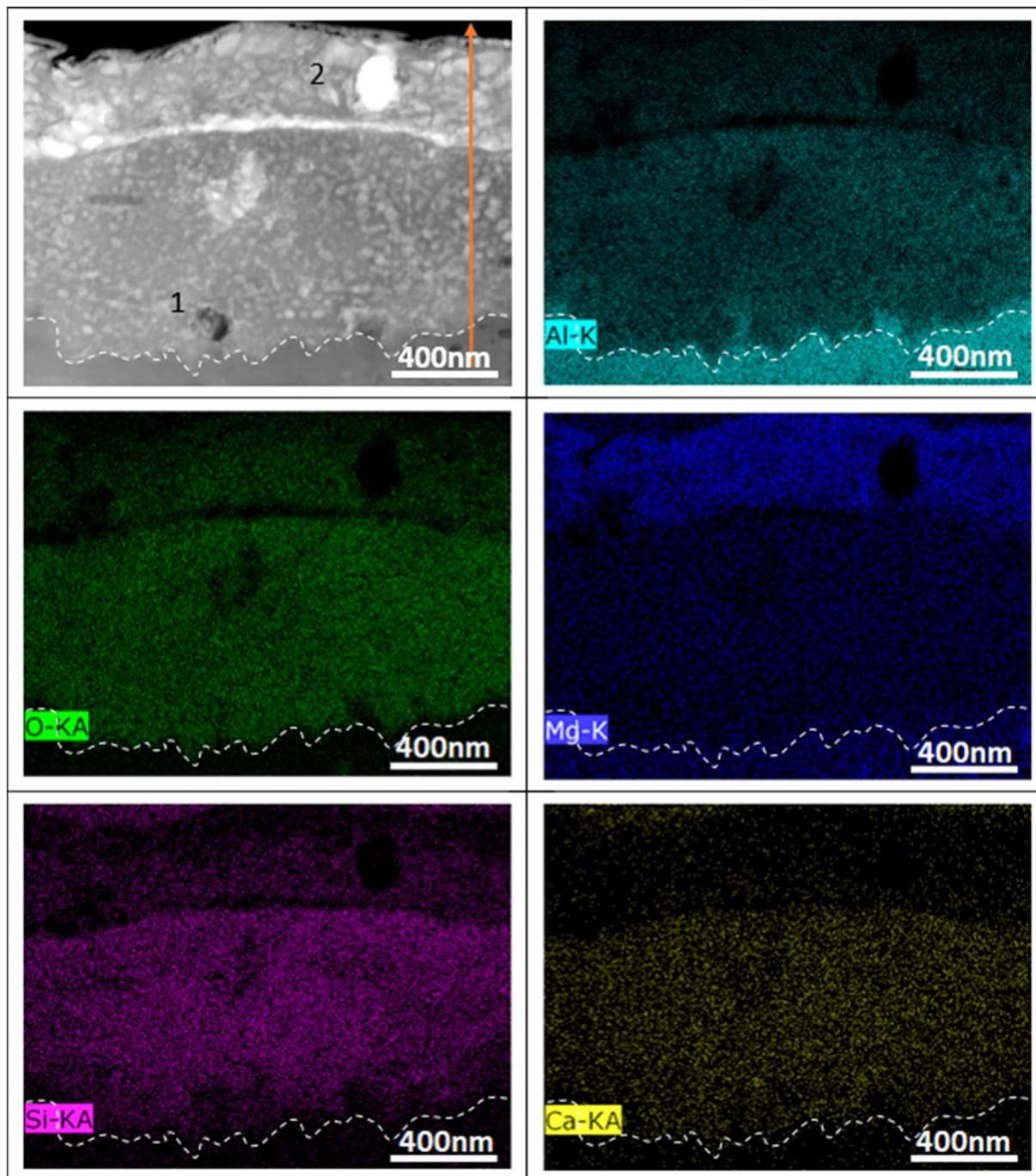


Figure 16 : EDX mapping of main elements present in the two-layered structure. On the TEM image, the zone indicated as 1 corresponds to an Fe-Mn inclusion and the zone indicated as 2 corresponds to a hole made in the outer layer by the electron beam during observation and analysis, due to its low porosity.

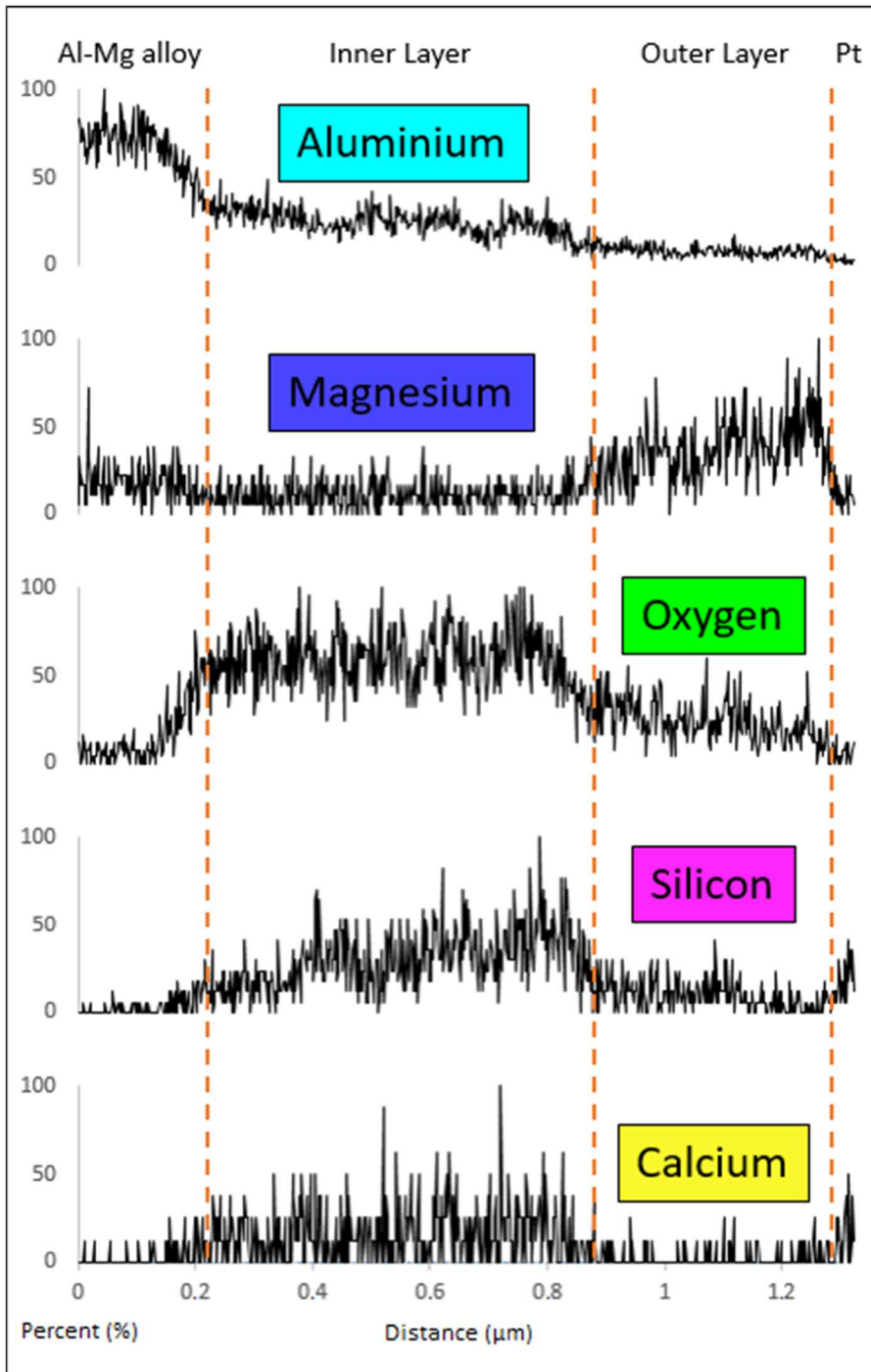


Figure 17 : EDX line scan of the main elements along the double-structure (orange arrow on the TEM image, Figure 16)

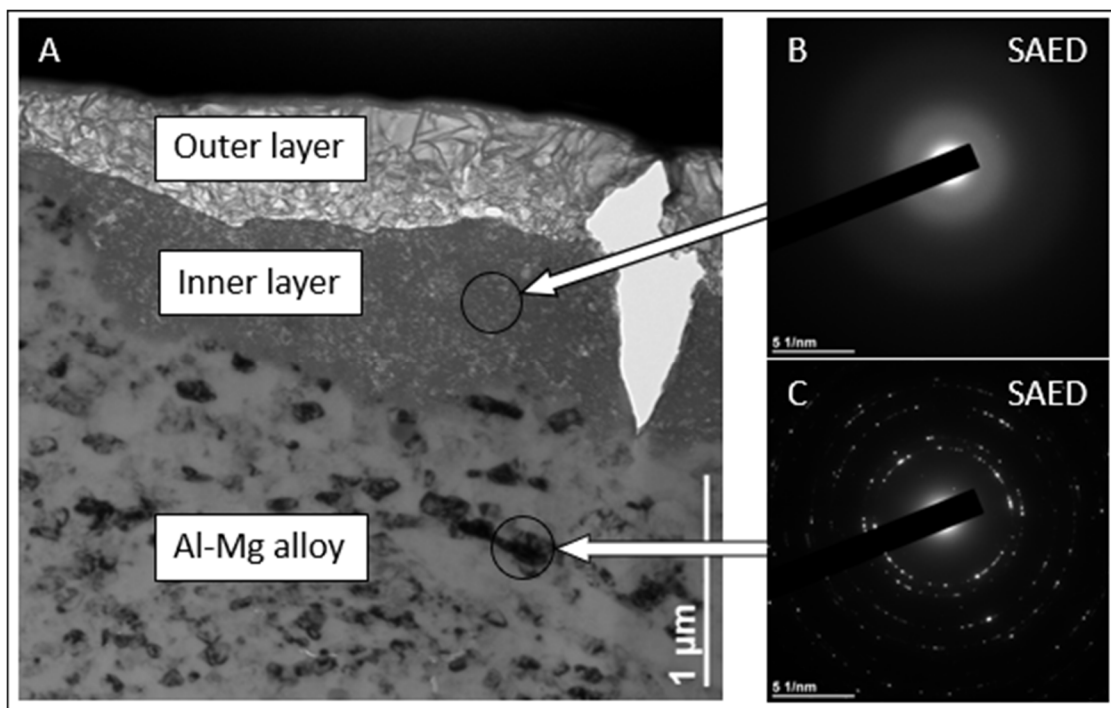


Figure 18 : Bright-field TEM image (A) and selected area electron diffraction patterns for the inner layer (B) and the Al-Mg alloy (C)

4. Discussion

Comparisons of the results in biotic and abiotic environments show that salt marsh microorganisms played a role in the surface modification of the aluminium alloy. Under the abiotic condition, the Al-Mg electrode was shown to be corroded (SEM surface and cross-section observations, Figure 5), with significant amounts of aluminium detected in the solution after the 50 days of immersion (ICP, Table 2). In biotic conditions, microorganisms interacted with the aluminium alloy to form a homogeneous layer on its surface, which was demonstrated to have a corrosion inhibiting effect (SEM cross-section observations, Figure 7). The amount of aluminium measured in solution for biotic condition 1 (ICP, Table 2) was about a quarter of that in the abiotic condition. A more detailed TEM characterization of the layer observed in biotic condition 1 verified that, despite its thickness of only about 1 micron, the layer presented a double-layer structure with elemental chemical composition differences in each (Figure 15).

An inner layer, denser and amorphous (Figure 18), showed excellent adhesion to the substrate and the amount of aluminium present in it was more significant than in the outer layer, which was more porous and significantly richer in magnesium (Figure 16 and Figure 17).

A decreasing gradient of aluminium content can be seen from the Al-Mg alloy to the outer layer (Figure 17). This suggests that the formation of the inner layer, adjacent to the Al-Mg surface, may be the result of a precipitation reaction between the Al dissolved from the Al-Mg alloy and the chemical elements present in the biotic solution, such as oxygen, silicon, and calcium. Functioning as a barrier to ion exchange, the inner layer would enable the development of a second layer, richer in magnesium and in direct contact with the medium.

The chemical elements identified in the double structure layer are the same as those also detected in some aluminum-based mineral compounds reported in the literature as having corrosion protection properties. Yang et al. presented a coating composed of α -Al₂O₃, γ -Al₂O₃, and 3Al₂O₃·2SiO₂ that improved the corrosion resistance of the magnesium alloys in 3.5 wt.% NaCl solution [38]. Al-Mg spinels, such as MgAl₂O₄/AlO_x and MgAl₂O₄/MgO_x obtained by several surface treatments on magnesium alloys have also proved to be resistant to corrosion in 0.5 M NaCl solution [39]. In the

present study, it is possible that similar layers could be produced by a biomineralization process using ions in solution and the microorganisms of the salt marsh. Silicon and magnesium are abundant in seawater and OH^- ions can be produced by oxygen reduction. The presence of calcium in the inner layer may also suggest the precipitation of calcium carbonate, which is consistent with the increase in pH as well as the presence of calcium in the medium. This biomineralization process could be an indirect, biologically-influenced mineralization (passive precipitation) but direct biologically-induced precipitation (active precipitation) is also possible [40]. Dupraz et al. proposed an active and passive precipitation mechanism for the formation of CaCO_3 precipitates. In the biofilm, a labile part of the EPS is constantly degraded, then renewed, and may allow the release of calcium bonds with the matrix, leading to active precipitation through the calcification of the biofilm. When the amount of calcium present exceeds the number of available bonds and the biofilm raises the pH of the medium through oxygen reduction, calcium precipitates, leading to passive precipitation [41]. The formation of CaCO_3 could also be caused by the consumption of organic matter by bacteria, producing CO_2 at a concentration allowing its precipitation with calcium, within the biofilm [42]. Salt marshes are known to form electroactive biofilms that are efficient for organic matter oxidation [43]. Shen et al. showed the formation of a $\text{CaMg}(\text{CO}_3)_2$ protective layer on the aluminium alloy, induced by using a single strain of *P. lipolytica* in seawater. In this case, the mechanism of the layer formation involved the large-scale production of EPS combined with the surrounding ions [25].

The layer with a double structure developed more effectively in biotic condition 1, with a medium containing salt marsh liquid and solids, than in biotic condition 2, with solid salt marsh only. Therefore, it can be asserted that the liquid part of the salt marsh contains the larger proportion of the microbial population responsible for this surface modification. Since this liquid part is exposed to the air, it contains more aerobic bacteria such as *Thiohalobacter thiocyanaticus* that can catalyze the oxygen reduction, as reported in [34] on a carbon surface. This catalytic phenomenon is expected on the aluminium alloy here.

To sum up, on the one hand, the catalysis of the cathodic reaction involves a faster and more significant increase in pH, which modifies the environment in the immediate vicinity of the interface, promoting precipitation phenomena.

On the other hand, the catalysis of the cathodic reaction is accompanied by an acceleration of anodic reactions on the same surface. The high corrosion current observed during the first 5 days in biotic conditions (Figure 4) is correlated with the increase of the aluminium dissolution (anodic reaction). Thus, this dissolved aluminium present in the vicinity of the sample could be concentrated enough to precipitate with other chemical elements present in the liquid medium [44] (abiotic reaction) or be used by bacteria to form the double layer structure on the Al-Mg surface.

In brief, seawater contains naturally high concentrations of calcium, magnesium and silicon and, near the alloy surface, the quantity of aluminium dissolved and the pH values are sufficient to lead to the precipitation of the observed protective layer through biomineralization mechanisms. Given the microbial diversity of the salt marsh, it is possible that several of the above mechanisms are involved.

5. Conclusion

Results presented in this paper show that microorganisms present in the salt marsh lead to the formation of a layer on an aluminium alloy surface in seawater, which ultimately protects against further corrosion. A detailed cross section characterization by TEM was used to verify that this layer had a double layer structure, composed of a dense, amorphous inner layer, whose elemental chemical composition indicates a probable inorganic nature, and a more porous outer layer, whose behavior and elemental chemical composition seem to suggest an inorganic-organic hybrid nature, which has not previously been demonstrated to our knowledge. However, aluminium alloy immersed in seawater with abiotic salt marsh was corroded and did not demonstrate the formation of the protective layer.

This work shows how MICI can be a source of inspiration for the development of more environmentally friendly technologies to produce effective anticorrosion coatings. The objective would be to reproduce

this coating by biomimicry, in order to substitute surface treatments currently used. Indeed, various treatments are used to protect aluminium alloys in an aggressive marine environment but they all have major drawbacks. Conversion treatments are generally based on chromium, which is prohibited in Europe; anodizing involves high energy costs; the use of organic coatings induces pollution; and cathodic protection releases zinc ion. The corrosion protection induced by MICI presented in this study has no such drawbacks and would offer new opportunities for more sustainable treatments.

6. Acknowledgments

This work was financially supported by the MESRI (Ministère de l'Enseignement Supérieur, de la Recherche et de l'Innovation) funding of the French government. This work was included in the MICOATEC project (ANR-19-CE08-0018) financially supported by the ANR.

7. Data availability statement

The raw/processed data required to reproduce these findings cannot be shared at this time as the data also forms part of an ongoing study.

8. References

- [1] R. Develay, Propriétés de l'aluminium et des alliages d'aluminium corroyés, Techniques de l'Ingénieur. Base documentaire : TIB357DUO. (1992). <https://www.techniques-ingenieur.fr/base-documentaire/materiaux-th11/metaux-et-alliages-non-ferreux-42357210/proprietes-de-l-aluminium-et-des-alliages-d-aluminium-corroyes-m440/>.
- [2] C. Vargel, Corrosion of Aluminium (2nd Edition), Elsevier, 2020.
- [3] R.T. Vashi, H.K. Kadiya, Corrosion Study of Metals in Marine Environment, E-Journal of Chemistry. 6 (2009) 1240–1246. <https://doi.org/10.1155/2009/509216>.
- [4] M.C. Reboul, T. Warner, H. Mayet, B. Baroux, A Ten-Step Mechanism for the Pitting Corrosion of Aluminium, Materials Science Forum. 217–222 (1996) 1553–1558. <https://doi.org/10.4028/www.scientific.net/MSF.217-222.1553>.
- [5] F. Guan, X. Zhai, J. Duan, J. Zhang, K. Li, B. Hou, Influence of sulfate-reducing bacteria on the corrosion behavior of 5052 aluminum alloy, Surface and Coatings Technology. 316 (2017) 171–179. <https://doi.org/10.1016/j.surfcoat.2017.02.057>.
- [6] H.-C. Flemming, J. Wingender, The biofilm matrix, Nature Reviews Microbiology. 8 (2010) 623–633. <https://doi.org/10.1038/nrmicro2415>.
- [7] M.A. Ghannoum, M.R. Parsek, M. Whiteley, P.K. Mukherjee, eds., Microbial biofilms, Second edition, ASM Press, Washington D.C, 2015.
- [8] I. Beech, A. Bergel, A. Mollica, H.-C. Flemming, V. Scotto, W. Sand, Simple methods for the investigation of the role of biofilms in corrosion, Brite-Euram Thematic Network on MIC of Industrial Materials. (2000).
- [9] R. Javaherdashti, Microbiologically Influenced Corrosion, Springer London, London, 2008. <https://doi.org/10.1007/978-1-84800-074-2>.
- [10] B.J. Little, D.J. Blackwood, J. Hinks, F.M. Lauro, E. Marsili, A. Okamoto, S.A. Rice, S.A. Wade, H.-C. Flemming, Microbially influenced corrosion—Any progress?, Corrosion Science. 170 (2020) 108641. <https://doi.org/10.1016/j.corsci.2020.108641>.
- [11] J. Telegdi, A. Shaban, L. Trif, Review on the microbiologically influenced corrosion and the function of biofilms, International Journal of Corrosion and Scale Inhibition. 9 (2020). <https://doi.org/10.17675/2305-6894-2020-9-1-1>.
- [12] S. Parot, I. Vandecandelaere, A. Cournet, M.-L. Délia, P. Vandamme, M. Bergé, C. Roques, A. Bergel, Catalysis of the electrochemical reduction of oxygen by bacteria isolated from electro-active biofilms formed in seawater, Bioresource Technology. 102 (2011) 304–311. <https://doi.org/10.1016/j.biortech.2010.06.157>.

- [13] R. Basséguy, M.-L. Délia, B. Erable, A. Bergel, Electroactive biofilms, in: *Understanding Biocorrosion*, Elsevier, 2014: pp. 107–143. <https://doi.org/10.1533/9781782421252.1.107>.
- [14] E. Zhou, H. Li, C. Yang, J. Wang, D. Xu, D. Zhang, T. Gu, Accelerated corrosion of 2304 duplex stainless steel by marine *Pseudomonas aeruginosa* biofilm, *International Biodeterioration & Biodegradation*. 127 (2018) 1–9. <https://doi.org/10.1016/j.ibiod.2017.11.003>.
- [15] B. Erable, I. Vandecandelaere, M. Faimali, M.-L. Delia, L. Etcheverry, P. Vandamme, A. Bergel, Marine aerobic biofilm as biocathode catalyst, *Bioelectrochemistry*. 78 (2010) 51–56. <https://doi.org/10.1016/j.bioelechem.2009.06.006>.
- [16] Y. Zhang, Y. Ma, J. Duan, X. Li, J. Wang, B. Hou, Analysis of marine microbial communities colonizing various metallic materials and rust layers, *Biofouling*. 35 (2019) 429–442. <https://doi.org/10.1080/08927014.2019.1610881>.
- [17] J.S. de Andrade, M.R.S. Vieira, S.H. Oliveira, S.K. de Melo Santos, S.L. Urtiga Filho, Study of microbiologically induced corrosion of 5052 aluminum alloy by sulfate-reducing bacteria in seawater, *Materials Chemistry and Physics*. 241 (2020) 122296. <https://doi.org/10.1016/j.matchemphys.2019.122296>.
- [18] B.M. Rosales, M. Iannuzzi, Aluminium AA2024 T351 aeronautical alloy, *Materials Science and Engineering: A*. 472 (2008) 15–25. <https://doi.org/10.1016/j.msea.2007.06.079>.
- [19] J.S. Lee, J.M. McBeth, R.I. Ray, B.J. Little, D. Emerson, Iron cycling at corroding carbon steel surfaces, *Biofouling*. 29 (2013) 1243–1252. <https://doi.org/10.1080/08927014.2013.836184>.
- [20] A. Al-Hashem, J.A. Carew, A. Al Borno, Screening Test for Six Dual Biocide Regimes against Planktonic and Sessile Populations of Bacteria, in: *NACE-04748, CORROSION 2004*, New Orleans, Louisiana, 2004.
- [21] N. Kip, J.A. van Veen, The dual role of microbes in corrosion, *The ISME Journal*. 9 (2015) 542–551. <https://doi.org/10.1038/ismej.2014.169>.
- [22] A. Nagiub, F. Mansfeld, Microbiologically influenced corrosion inhibition (MICI) due to bacterial contamination, *Materials and Corrosion*. 52 (2001) 817–826. [https://doi.org/10.1002/1521-4176\(200111\)52:11<817::AID-MACO817>3.0.CO;2-1](https://doi.org/10.1002/1521-4176(200111)52:11<817::AID-MACO817>3.0.CO;2-1).
- [23] C. Cote, O. Rosas, R. Basseguy, *Geobacter sulfurreducens*: An iron reducing bacterium that can protect carbon steel against corrosion?, *Corrosion Science*. 94 (2015) 104–113. <https://doi.org/10.1016/j.corsci.2015.01.044>.
- [24] M.S. Suma, R. Basheer, B.R. Sreelekshmy, V. Vipinlal, M.A. Sha, P. Jineesh, A. Krishnan, S.R. Archana, V.S. Saji, S.M.A. Shibli, *Pseudomonas putida* RSS biopassivation of mild steel for long term corrosion inhibition, *International Biodeterioration & Biodegradation*. 137 (2019) 59–67. <https://doi.org/10.1016/j.ibiod.2018.11.008>.
- [25] Y. Shen, Y. Dong, Y. Yang, Q. Li, H. Zhu, W. Zhang, L. Dong, Y. Yin, Study of pitting corrosion inhibition effect on aluminum alloy in seawater by biomineralized film, *Bioelectrochemistry*. 132 (2020) 107408. <https://doi.org/10.1016/j.bioelechem.2019.107408>.
- [26] A. Jayaraman, E. Cheng, J. Earthman, T. Wood, Axenic aerobic biofilms inhibit corrosion of SAE 1018 steel through oxygen depletion, *Applied Microbiology and Biotechnology*. 48 (1997) 11–7. <https://doi.org/10.1007/s002530051007>.
- [27] V.S. Sinyavskii, V.D. Kalinin, Marine Corrosion and Protection of Aluminum Alloys According to Their Composition and Structure, *Protection of Metals*. 41 (2005) 317–328. <https://doi.org/10.1007/s11124-005-0046-8>.
- [28] E. Juzeliūnas, R. Ramanauskas, A. Lugauskas, K. Leinartas, M. Samulevičienė, A. Sudavičius, Influence of wild strain *Bacillus mycoides* on metals: From corrosion acceleration to environmentally friendly protection, *Electrochimica Acta*. 51 (2006) 6085–6090. <https://doi.org/10.1016/j.electacta.2006.01.067>.
- [29] M.J.F. Marques, I.N. Alves, R.P. Gonçalves, T.C. Diamantino, AA 5083 Al Alloy Corrosion in Estuarine Environment, in: *Poster at Eurocorr 2013*, Estoril, Portugal, 2013.
- [30] M.J.F. Marques, G. Pavanello, T.C. Diamantino, M. Faimali, R. Basséguy, Influence of microbial activity on Al Alloys in marine medium: natural vs artificial seawater, in: *Oral Presentation at Eurocorr 2017*, Prague, Czech Republic, 2017.

- [31] M.J.F. Marques, T.C. Diamantino, R. Basséguy, Assessment of Anticorrosion Properties of Biomineralized Induced Coating formed on Al Alloy in Marine Environment. A new Nature-Inspired Approach for Corrosion Protection., in: Oral Presentation at Eurocorr 2020, 2020.
- [32] R. Rousseau, Production de biohydrogène par électro-catalyse microbienne, Institut national polytechnique de Toulouse, 2013. <http://www.theses.fr/2013INPT0150/document>.
- [33] H. Jianyu, L. Xuezhu, Z. Rongtao, W. Fangwei, W. Jianxin, Diversity of cultured and uncultured bacteria in surface layer sediment from the East China Sea: Diversity of cultured and uncultured bacteria in surface layer sediment from the East China Sea, *Biodiversity Science*. 21 (2013) 28–37. <https://doi.org/10.3724/SP.J.1003.2013.10097>.
- [34] M. Rimboud, M. Barakat, W. Achouak, A. Bergel, M.-L. Délia, Oxygen-reducing microbial cathodes in hypersaline electrolyte, *Bioresource Technology*. 319 (2020) 124165. <https://doi.org/10.1016/j.biortech.2020.124165>.
- [35] R. Rousseau, C. Santaella, W. Achouak, J.-J. Godon, A. Bonnafous, A. Bergel, M.-L. Délia, Correlation of the Electrochemical Kinetics of High-Salinity-Tolerant Bioanodes with the Structure and Microbial Composition of the Biofilm, *ChemElectroChem*. 1 (2014) 1966–1975. <https://doi.org/10.1002/celec.201402153>.
- [36] AFNOR, BS EN 573-3:2019 E. Aluminium and aluminium alloys - Chemical composition and form of wrought products, (2019). <https://www.boutique.afnor.org/standard/bs-en-573-32019/aluminium-and-aluminium-alloys-chemical-composition-and-form-of-wrought-products-chemical-composition-and-form-of-products/article/932658/eu160328>.
- [37] M. Faimali, E. Chelossi, G. Pavanello, A. Benedetti, I. Vandecandelaere, P. De Vos, P. Vandamme, A. Mollica, Electrochemical activity and bacterial diversity of natural marine biofilm in laboratory closed-systems, *Bioelectrochemistry*. 78 (2010) 30–38. <https://doi.org/10.1016/j.bioelechem.2009.04.012>.
- [38] S. Yang, L. Zhou, X. Cheng, Micro-Arc Oxide Film of Aluminum Coating Pre-Sprayed on AZ31 Magnesium Alloy, in: A. Singh, K. Solanki, M.V. Manuel, N.R. Neelameggham (Eds.), *Magnesium Technology 2016*, John Wiley & Sons, Inc., Hoboken, NJ, USA, 2016: pp. 291–295. <https://doi.org/10.1002/9781119274803.ch57>.
- [39] M. Tacikowski, P. Kobus, J. Kamiński, B. Kucharska, K. Kulikowski, P. Marchlewski, M. Pisarek, Structure and properties of composite aluminum oxide layers produced on magnesium alloys using hybrid method, *Vacuum*. 160 (2019) 325–332. <https://doi.org/10.1016/j.vacuum.2018.11.044>.
- [40] C. Dupraz, R.P. Reid, O. Braissant, A.W. Decho, R.S. Norman, P.T. Visscher, Processes of carbonate precipitation in modern microbial mats, *Earth-Science Reviews*. 96 (2009) 141–162. <https://doi.org/10.1016/j.earscirev.2008.10.005>.
- [41] C. Dupraz, P.T. Visscher, L.K. Baumgartner, R.P. Reid, Microbe-mineral interactions: early carbonate precipitation in a hypersaline lake (Eleuthera Island, Bahamas): Microbe-mineral interactions, Eleuthera Island, Bahamas, *Sedimentology*. 51 (2004) 745–765. <https://doi.org/10.1111/j.1365-3091.2004.00649.x>.
- [42] Z. Guo, S. Pan, T. Liu, Q. Zhao, Y. Wang, N. Guo, X. Chang, T. Liu, Y. Dong, Y. Yin, *Bacillus subtilis* Inhibits *Vibrio natriegens*-Induced Corrosion via Biomineralization in Seawater, *Frontiers in Microbiology*. 10 (2019) 1111. <https://doi.org/10.3389/fmicb.2019.01111>.
- [43] R. Rousseau, M. Rimboud, M.-L. Délia, A. Bergel, R. Basséguy, Electrochemical characterization of microbial bioanodes formed on a collector/electrode system in a highly saline electrolyte, *Bioelectrochemistry*. 106 (2015) 97–104. <https://doi.org/10.1016/j.bioelechem.2015.06.011>.
- [44] C.T. Driscoll, W.D. Schecher, The chemistry of aluminum in the environment, *Environmental Geochemistry and Health*. 12 (1990) 28–49. <https://doi.org/10.1007/BF01734046>.

Figure captions

Figure 1 : Different immersion conditions

Figure 2 : Experimental setup of the three-electrode system

Figure 3 : Open circuit potential (OCP) recorded during 50 days of immersion for biotic condition 1 (green dashes), biotic condition 2 (red dots) and abiotic condition (blue solid line)

Figure 4 : Evolution of $1/R_p$ during 50 days of immersion for biotic condition 1 (green dashes), biotic condition 2 (red dots) and abiotic condition (blue solid line)

Figure 5 : Photographs of aluminium alloy before and after 50 days of immersion in various conditions

Figure 6 : Surface SEM observation of a sample immersed in **biotic** condition 1

Figure 7 : Cross-sectional SEM observation of a sample immersed for 50 days with **biotic** condition 1. A and B reflect areas with less roughness than D. Framed areas on image D were analyzed by EDX and associated spectra are grouped in Figure 8

Figure 8 : EDX analysis of the sample in biotic condition 1, for areas framed in Figure 7D: zone 1 (Layer), zone 2 (Matrix of Al-Mg alloy) and zone 3 (Intermetallic particles)

Figure 9 : Surface SEM observation of a sample immersed in **biotic** condition 2.

Figure 10 : Cross-sectional SEM observation of a sample immersed for 50 days with **biotic** condition 2. Images A and B show the shape of the layer, while images C and D reveal a defect in this layer. Areas indicated by crosses on image D were analyzed by EDX.

Figure 11 : EDX analysis of the sample in **biotic** condition 2, Figure 10D, spectrum at cross 1 (Layer) and spectrum at cross 2 (Corroded area)

Figure 12 : Surface SEM observation of a sample immersed in **abiotic** condition

Figure 13 : Cross-sectional SEM observation of a sample immersed for 50 days in **abiotic** condition. A and C show corrosion at the surface of the aluminium alloy. The framed area on image D was analyzed by EDX.

Figure 14 : EDX analysis of the sample immersed in **abiotic** condition, on the framed zone of Figure 13D

Figure 15 : Cross-sectional bright-field TEM image of the layer formed at the Al-Mg electrode surface after 50 days of immersion in biotic condition 1. (A) Detail showing a two-layer structure: an inner dense layer and outer porous layer (B).

Figure 16 : EDX mapping of main elements present in the two-layered structure. On the TEM image, the zone indicated as 1 corresponds to an Fe-Mn inclusion and the zone indicated as 2 corresponds to a hole made in the outer layer by the electron beam during observation and analysis, due to its low porosity.

Figure 17 : EDX line scan of the main elements along the double-structure (orange arrow on the TEM image, Figure 16)

Figure 18 : Bright-field TEM image (A) and selected area electron diffraction patterns for the inner layer (B) and the Al-Mg alloy (C)

Table captions

Table 1 : Elemental composition (wt%) of samples from the 5083alloy and comparison with Standard EN 573

Table 2 : Dissolved aluminium analyzed by ICP-AES in the seawater after 50 days of immersion.